

# Self-supervised prior learning improves structured illumination microscopy resolution

Ze-Hao Wang<sup>†1,2</sup>, Tong-Tian Weng<sup>†1,2</sup>, Long-Kun Shan<sup>1,2</sup>, Xiang-Dong Chen<sup>1,2</sup>,  
Guang-Can Guo<sup>1,2</sup>, Fang-Wen Sun<sup>†\*1,2</sup>, and Tian-Long Chen<sup>†\*3,4</sup>

<sup>1</sup>CAS Key Laboratory of Quantum Information, University of Science and Technology of China, Hefei 230026, China.

<sup>2</sup>CAS Center for Excellence in Quantum Information and Quantum Physics, University of Science and Technology of China, Hefei 230026, China.

<sup>3</sup>Computer Science and Artificial Intelligence Laboratory, Massachusetts Institute of Technology, Massachusetts 02139, United States.

<sup>4</sup>Department of Biomedical Informatics, Harvard University, Massachusetts 02138, United States.

## Abstract

Structured illumination microscopy (SIM) is a wide-field super-resolution technique normally limited to roughly twice the diffraction-limited resolution ( $\approx 100\text{--}200$  nm). Surpassing this bound is a classic ill-posed inverse problem: recovering high-frequency structure from band-limited raw data. We introduce SIMFormer, a fully blind SIM reconstruction framework that learns a powerful, data-driven prior directly from raw images via self-supervision. This learned prior regularizes the solution and enables reliable extrapolation beyond the optical transfer function cutoff, yielding an effective resolution of approximately 45 nm. We validate SIMFormer on synthetic data and the BioSR dataset, where it resolves features such as flattened endoplasmic reticulum lipid bilayers previously reported to require STORM-level resolution. A self-distilled variant, SIMFormer+, further improves noise robustness while preserving high resolution at extremely low photon counts. These results show that learned priors can substantially extend SIM resolution and robustness, enabling rapid, large-scale imaging with STORM-level detail.

**One-sentence summary.** By using a self-supervised learned prior to address the ill-posed nature of image reconstruction, SIMFormer achieves 45 nm resolution in structured illumination microscopy, revealing endoplasmic reticulum details with a clarity previously requiring STORM-level techniques.

## Introduction

In the field of super-resolution imaging, various methods such as stimulated emission depletion microscopy (STED) [1], stochastic optical reconstruction microscopy (STORM) [2], and photoactivated localization microscopy (PALM) [3] have greatly enhanced resolution beyond the diffraction limit. Among them, structured illumination microscopy (SIM) [4] is widely adopted because of its

---

These authors contributed equally to this work.

These authors jointly supervised this work.

Email: fwsun@ustc.edu.cn, tianlong@mit.edu.

fast imaging speed, wide field of view, and relatively simple optical setup. SIM relies on computational reconstruction to extend the optical transfer function (OTF) by projecting structured light patterns onto a sample. This process encodes high-frequency sample information into detectable low-frequency moiré fringes, conventionally doubling the microscope’s native resolution.

Achieving resolution beyond this twofold enhancement presents a classic ill-posed inverse problem [5]. Because the raw data are band-limited by the system’s OTF, there are infinitely many high-resolution structures that could produce the same observed low-resolution image. To determine a unique and physically plausible solution, one must introduce additional constraints, or prior knowledge, about the sample’s structure [6–8]. Advanced algorithms have incorporated handcrafted priors, such as sparsity and continuity, to improve resolution [9], but these priors can be overly simplistic and sensitive to parameter tuning, limiting their generalizability in practice [10].

The deep learning revolution inspired a shift toward data-driven, learnable priors that utilize deep neural networks trained with labeled data for SIM reconstruction [11]. Notable supervised approaches include U-Net-SIM [12], DF-CAN [13], and related variants that learn a direct mapping from diffraction-limited or conventionally reconstructed SIM images to super-resolved outputs. However, the practical application of such supervised methods is highly limited by their poor generalization ability when applied to new, unseen testing samples, particularly when the training and test distributions differ in fluorophore density, optical properties, or imaging conditions [11]. These out-of-distribution generalization issues lead to hallucinations and artifacts, thereby impeding robust generalization in microscopic imaging [11].

Here we introduce SIMFormer, a Transformer-based [14, 15] self-supervised learning framework that resolves the ill-posed challenge of SIM reconstruction by learning a powerful, data-driven prior directly from raw microscopy data. Using a masked autoencoder (MAE) training strategy [16, 17], SIMFormer is compelled to learn the intrinsic statistical patterns of biological structures. This learned prior acts as a sophisticated, adaptive regularizer, guiding the reconstruction to solutions that are not only consistent with the measured low-frequency data but also conform to the learned characteristics of plausible biological structures.

Such a process can be viewed as reliable spectral extrapolation, in which the network leverages the available low-frequency information and the strong data-driven prior to infer the most probable high-frequency information that was not directly measured. Consequently, SIMFormer achieves a resolution of approximately 45 nm—nearly a fivefold improvement over the diffraction limit. The framework is fully blind, simultaneously estimating the emitters, illumination patterns, background, and point spread function (PSF) from the raw data alone. To further enhance noise robustness under low-photon-count conditions, we introduce SIMFormer+, a refined model developed through self-distillation [18–21]. The effectiveness of SIMFormer is thoroughly validated through extensive evaluations on both synthetic and real-world SIM datasets, including the BioSR benchmark [13], which comprises diverse biological structures such as clathrin-coated pits (CCPs), endoplasmic reticula (ER), microtubules (MTs), and F-actin filaments. Together, these results highlight the broad applicability and practical utility of SIMFormer for super-resolution fluorescence imaging.

## Results

### Prior learning via low-dimensional subspace projection in SIMFormer

Conventional maximum a posteriori (MAP) image reconstruction methods address ill-posedness by incorporating explicit, handcrafted priors such as sparsity and smoothness to regularize the solution [6–8]. In contrast, SIMFormer utilizes learnable priors that emerge from the data itself through the use of MAE [16, 22]. By reconstructing images from aggressively masked inputs, often

discarding around 75% of patches during training, MAE is compelled to capture only the most predictive feature components from the visible patches. This masking-driven process confines the representation to a task-driven, data-adaptive, low-dimensional subspace, effectively creating an implicit prior learned directly from the training data without requiring any manual assumptions on emitters [22]. One can formulate the MAE objective in MAP terms as minimizing a reconstruction error with a learned regularizer, where the reconstruction network operates on the target image and the regularizer encodes the learned prior on the latent code.

In SIMFormer, this low-dimensional subspace acts as a powerful prior that constrains the solution to biologically plausible structures. Because the encoder must consistently reconstruct masked regions from the context of unmasked patches, it learns to capture structural regularities such as filament continuity, tubular topology, and network connectivity. These features are precisely the kinds of information needed to disambiguate multiple high-frequency solutions compatible with the same band-limited data. As a result, SIMFormer performs reliable spectral extrapolation while avoiding hallucinations that conflict with the statistics of its training data.

### Comparison with existing methods

SIMFormer’s approach to generating and utilizing priors fundamentally distinguishes it from other SIM reconstruction methods. Traditional algorithms such as Sparse-SIM [9] and Blind-SIM [23] depend on iterative optimization guided by explicit, handcrafted priors and parametric assumptions about the illumination pattern. These non-learning methods are often computationally intensive and sensitive to parameter tuning [10]. Recent deep learning approaches operate on varied principles. Some, such as the Swin Transformer-based denoising method by Shah *et al.* [24] and the self-supervised multimodal denoising method by Chen *et al.* [25], are post-process denoisers applied to previously reconstructed images; consequently, they cannot recover spatial frequencies lost during initial reconstruction. Others, for instance, the physics-informed network by Burns and Liu [26], perform end-to-end reconstruction using an untrained network’s implicit prior. These physics-informed methods typically require known illumination patterns and remain bound by the theoretical  $2\times$  resolution limit.

SIMFormer, in contrast, is a full, end-to-end blind reconstruction engine that leverages a strong, data-driven prior learned through self-supervision. This learned prior functions as an adaptive regularizer, allowing for reliable spectral extrapolation beyond conventional resolution limits. Unlike handcrafted priors that must be manually tuned for different structures and imaging conditions, the learned prior in SIMFormer emerges directly from raw training data and adapts to complex biological structures. Moreover, by jointly estimating emitters, patterns, background, and PSF, SIMFormer is able to account for experimental imperfections that are hard to model analytically, such as deviations from ideal sinusoidal illumination and subtle aberrations in the PSF.

### Network architecture of SIMFormer

SIMFormer introduces a novel architecture for fully blind SIM reconstruction with four main components.

(1) *Data processor*: Raw SIM images are taken as an input stack consisting of three phases from each of three SIM directions. The input stack is divided into  $3 \times 16 \times 16$  3D cubes, which are transformed into 768-dimensional vectors by patch embedding.

(2) *Encoder*: The embedded data are processed by a Transformer encoder derived from ViT [15] (ViT-base) with 12 Transformer layers. To accelerate training and improve dense prediction capabilities, we introduce an adapter module into the encoder [27]. The encoder is initialized by

CLIP-based pre-training [28] to leverage large-scale natural image representations and improve optimization stability.

(3) *Decoder*: The encoded features are processed by a decoder with multiple Transformer layers. The decoder output is passed through three convolutional decoding heads to separately reconstruct emitters, light patterns, and background, which together synthesize the raw SIM images. For the light pattern, a low-rank coding module is introduced before the convolutional decoder head to progressively compress the rank of the light pattern representation during training, reflecting the prior knowledge that only a few pattern modes are physically present.

(4) *PSF branch*: The PSF is modeled by feeding a fixed random embedding to a learnable convolutional neural network, following the philosophy of deep image priors [29, 30]. Overall, the raw SIM images are synthesized using the emitters, light patterns, background, and PSF according to the physical principles of SIM imaging.

The entire pipeline (Fig. 1) is trained in a self-supervised manner: the network takes raw SIM stacks as input and predicts emitters, patterns, background, and PSF whose forward simulation must match the original raw stacks. This design tightly couples the learned prior with a physically realistic forward model.

## Multi-stage self-supervised training

Our SIMFormer adopts a multi-stage self-supervised training approach inspired by curriculum learning [31]. At each stage, the masking rate and the compression ratio of the low-rank coding are adjusted: the masking rate decreases, while the compression ratio gradually increases, following a multi-stage schedule. This design aims to prevent the model from converging to trivial PSF solutions in the early stages and to promote a stable progression toward low-rank coding for the light pattern.

The training objective consists of four parts: (1) a reconstruction loss measuring the difference between synthesized and raw SIM images; (2) a total variation loss enforcing smoothness in the predicted light pattern; (3) a total variation loss for the PSF to encourage smooth, physically plausible responses; and (4) a mean absolute error loss enforcing alignment between the PSF centroid and the image center. A weighted combination of  $L_1$  and MS-SSIM terms is used for image fidelity, as is common in image restoration networks [32]. Details are provided in the Materials and Methods section.

## Self-distillation and SIMFormer+

Knowledge distillation [19] trains a student model to replicate the behavior of a teacher model. We adopt a self-distillation approach [18, 20, 21], where the student model shares the same architecture as the teacher. Using the teacher’s predictions as soft labels, the student model refines and enhances the original outputs, resulting in improved accuracy and stronger noise robustness. This refined model is referred to as SIMFormer+.

Specifically, SIMFormer is first trained on high-SNR SIM images, producing high-resolution predictions. These predictions are then used as pseudo ground truth to supervise SIMFormer+ at lower photon counts and higher noise levels. By matching the teacher’s soft predictions rather than hard labels, the student model learns to preserve fine structures while being explicitly optimized for robustness under challenging noise conditions. As a result, SIMFormer+ inherits the teacher’s high-resolution capabilities while substantially improving robustness to photon starvation and detector noise.

## Data preparation

We demonstrate SIMFormer’s capabilities using both synthetic and real-world data. For synthetic validation, several datasets with varying fluorophore structures, light pattern spatial periods, noise levels, line sparsity, tube widths, and ring radii are generated. In these datasets, the fluorescence wavelength is set to 488 nm, the objective numerical aperture (NA) is 1.3, and the pixel size is 62.6 nm. The PSF is simulated using a vectorial Debye integral model, corresponding to a diffraction limit of 229 nm. The light pattern is modeled as a cosine function oriented in three directions with three phases per direction. Using the emitters, light patterns, and PSF, we synthesize raw SIM images and reconstruct super-resolution images using a conventional algorithm (Supplementary Notes 2 and 3). For each parameter configuration, we generate 100 training samples and 100 test samples.

For real-world validation, we adopt the BioSR dataset [13], which contains raw SIM images of various biological structures, including CCPs, ER, MTs, and F-actin, along with the corresponding super-resolution images obtained through conventional SIM reconstruction. This dataset covers a wide range of structural densities and morphologies, providing a stringent test for reconstruction algorithms.

## Comparative evaluation and metrics

We evaluate SIMFormer using both synthetic and real experimental data and compare it with conventional SIM reconstruction, Sparse-SIM [9], and Blind-SIM [23]. Sparse-SIM is currently one of the state-of-the-art SIM reconstruction algorithms with high resolution [9], while Blind-SIM is a widely used blind reconstruction algorithm [23]. Using the labeled synthetic dataset, we examine the superiority of SIMFormer over Sparse-SIM and Blind-SIM under two challenging conditions: (1) SIMFormer is trained and predicts in a fully blind manner, whereas Sparse-SIM has access to experimental parameters and Blind-SIM uses the true PSF; and (2) the performance of Sparse-SIM and Blind-SIM is fine-tuned using global optimization of their hyperparameters (Supplementary Note 4), whereas SIMFormer is not fully optimized due to computational resource limitations. In real-world experiments, Blind-SIM uses the same parameters as in the synthetic experiments, while Sparse-SIM employs new parameters (Supplementary Table 2).

The synthetic dataset provides actual emitters as ground truth, allowing the use of normalized root-mean-square error (NRMSE) and multiscale structural similarity index (MS-SSIM) to evaluate reconstructed images [32]. NRMSE quantifies overall intensity differences between predicted and actual images, while MS-SSIM assesses structural similarity across multiple scales. NRMSE with added Gaussian blur is used to measure spatial distance error of emitters (Supplementary Note 5). Since the resolution achieved by Sparse-SIM and SIMFormer surpasses conventional SIM reconstruction in the BioSR dataset (where no ground truth is available), we focus on discriminability of regions of interest and compare results with prior knowledge from STORM imaging of ERs [33]. Additionally, decorrelation analysis [34] is used to measure resolution (Supplementary Note 6). For noise robustness evaluation, we use fairSIM [35] to generate conventional SIM reconstructions under high noise, as these results are not available in BioSR.

## SIMFormer on synthetic data

We first evaluate SIMFormer on synthetic filament structures, where fluorophores are simulated using randomly generated curves based on Bessel functions (Supplementary Note 2). SIMFormer and SIMFormer+ substantially improve NRMSE and MS-SSIM compared with widefield imaging,

conventional SIM, Blind-SIM, and Sparse-SIM, and achieve significantly improved resolution according to decorrelation analysis [34]. Zoomed-in regions show that: (1) conventional SIM fails to resolve fine buckle structures; (2) Blind-SIM introduces significant artifacts; (3) Sparse-SIM shows fewer artifacts but still cannot distinctly resolve the structures; (4) SIMFormer produces plausible reconstructions with fewer artifacts; and (5) SIMFormer+ yields the clearest buckle structures owing to self-distillation improving robustness.

We then evaluate synthetic microtubule structures. SIMFormer and SIMFormer+ again outperform existing methods in both NRMSE and MS-SSIM, and achieve higher resolution than Blind-SIM and Sparse-SIM. In zoomed-in regions, microtubule structures narrower than the diffraction limit are resolved only by SIMFormer and SIMFormer+. Extended Data Fig. 2 shows that Sparse-SIM and Blind-SIM can resolve only wider microtubules, with Sparse-SIM performing relatively better than Blind-SIM.

Finally, we simulate ring-shaped fluorophores with varying radii. SIMFormer and SIMFormer+ again significantly improve NRMSE and MS-SSIM, and decorrelation analysis indicates that SIMFormer+ achieves about 2.8 times the resolution of conventional SIM and 1.5 times that of Blind-SIM and Sparse-SIM. SIMFormer and SIMFormer+ resolve ring structures of about 75 nm diameter, which conventional SIM, Sparse-SIM, and Blind-SIM do not. Extended Data Fig. 3 shows that Sparse-SIM resolves rings 125 nm or larger, while Blind-SIM resolves rings 165 nm or larger. Overall, considering discernibility, accuracy, and resolution, SIMFormer+ achieves the best performance across all synthetic tasks.

## SIMFormer on the BioSR dataset

We next use the BioSR dataset [13] to evaluate SIMFormer in real-world conditions. The dataset contains CCPs, ER, MTs, and F-actin filaments, covering structures from sparse to dense. With fluorescence wavelength 488 nm and NA 1.3, the diffraction limit is 229 nm. Raw SIM images are processed using Blind-SIM, Sparse-SIM, and SIMFormer, alongside conventional SIM reconstructions provided in BioSR. Self-distillation on SIMFormer results yields SIMFormer+.

Fig. 3 shows a side-by-side comparison of methods on BioSR. CCPs are ring-like assemblies of clathrin, typically 50–150 nm in diameter and essential for endocytosis [36]. SIMFormer is the only method that detects sub-100 nm micro-rings, while all methods detect larger rings; SIMFormer+ matches SIMFormer and further suppresses residual artifacts.

The ER forms a tubular network with 50–100 nm diameter tubules [33]. Sparse-SIM provides sharper, more coherent results than the conventional SIM reconstruction in BioSR but fails to resolve tubular structures; Blind-SIM shows some microtubules but with many artifacts. SIMFormer clearly reveals tubules consistent with STORM results, and SIMFormer+ further improves robustness and suppresses low-light artifacts (Extended Data Fig. 4).

MTs are 25 nm-diameter cytoskeletal polymers essential for structural support and intracellular transport [37]. All methods resolve filamentous structures, but SIMFormer provides clearer results in overlapping regions, with SIMFormer+ further reducing artifacts. Extended Data Fig. 5 demonstrates that SIMFormer can resolve microtubules significantly narrower than the diffraction limit.

F-actin filaments (about 7 nm in diameter) form dense cytoskeletal networks [38]. SIMFormer resolves these dense structures more clearly than other methods; SIMFormer+ further reduces artifacts in low-light regions (Supplementary Fig. 3). Resolution estimated by decorrelation analysis (Fig. 3e–h) shows that SIMFormer and SIMFormer+ reach average resolutions of 46.5 nm and 47.6 nm (4.9 and 4.8 times the diffraction limit), while conventional SIM reconstruction achieves around 1.7 times, Sparse-SIM about 2.3 times, and Blind-SIM about 3.1 times the diffraction limit

but with significant artifacts [34].

The practical power of SIMFormer’s learned prior is especially evident in its ability to resolve  $\sim 80$  nm ER tubules, a level of detail previously associated with STORM imaging [33]. This is not merely image enhancement but reliable spectral extrapolation beyond the conventional  $2\times$  resolution limit. The adaptive, data-driven prior overcomes the limitations of rigid handcrafted priors such as sparsity, which are ill-suited for complex, interconnected ER networks, and allows SIMFormer to infer high-frequency information inaccessible to traditional methods.

### Light pattern prediction and noise robustness

Trained by reconstructing raw SIM images, the accuracy of SIMFormer’s light pattern prediction is directly tied to the accuracy of its emitter predictions. We evaluate predicted light patterns on synthetic datasets and compare them to Blind-SIM. Due to learned priors and low-rank coding, SIMFormer’s predicted light patterns are significantly closer to the true ones, especially near emitters where light pattern accuracy matters most for reconstruction. On BioSR data, SIMFormer accurately predicts cosine-like light patterns across CCPs, ER, MTs, and F-actin, whereas Blind-SIM produces anomalous patterns (Fig. 4).

Noise robustness is validated using both synthetic and BioSR datasets. With varying average photon numbers, SIMFormer and SIMFormer+ consistently outperform other methods in NRMSE and MS-SSIM. SIMFormer+ greatly improves SIMFormer’s performance under extremely low photon counts, reducing NRMSE and maintaining consistent resolution where SIMFormer alone suffers from artifacts that hinder decorrelation analysis (Fig. 5 and Supplementary Figs. 4–7).

On BioSR, side-by-side comparisons under low and high photon counts show that SIMFormer and SIMFormer+ produce fewer artifacts and greater robustness across tasks, with SIMFormer+ consistently improving artifact suppression and structure discernibility (Fig. 6 and Extended Data Figs. 6–9).

## Discussion

We have presented SIMFormer, a fully blind reconstruction framework that simultaneously estimates sample structure, PSF, light patterns, and background from raw SIM images. By combining a self-supervised learned prior with low-rank encoding of the light pattern, SIMFormer achieves a resolution approaching 45 nm—nearly five times the diffraction limit—while significantly improving light pattern estimation accuracy over previous blind methods [9, 23]. With self-distillation, SIMFormer+ further enhances reconstruction accuracy and noise robustness without compromising resolution.

Conceptually, SIMFormer occupies an intermediate position between traditional MAP-based reconstruction and end-to-end supervised learning. Like MAP methods, it incorporates an explicit forward model of SIM imaging and uses this model to enforce consistency between predicted emitters, patterns, PSF, and raw data [6–8]. Unlike classical approaches, however, the regularizer is not a simple penalty such as sparsity or total variation; instead, it is an implicit prior encoded in the encoder–decoder network and learned directly from raw microscopy data via self-supervised training [16, 17]. This design allows SIMFormer to adapt to complex biological structure statistics and to extrapolate beyond the nominal OTF cutoff, while maintaining robustness to experimental variability.

Compared with purely data-driven supervised approaches [11–13], SIMFormer avoids the need for large paired datasets of low- and high-resolution images, which are difficult or impossible to obtain for many biological preparations. Instead, it relies only on raw SIM stacks and a physically

motivated forward model. This greatly simplifies data acquisition and makes the framework more amenable to deployment in diverse laboratories. Furthermore, because the forward model remains explicit, SIMFormer’s behavior is easier to interpret and diagnose than that of black-box image-to-image networks.

SIMFormer also demonstrates how learned priors and physical models can be tightly integrated. The architecture is deliberately structured so that each predicted component (emitters, patterns, background, PSF) has a clear physical interpretation, and each is regularized in a way that reflects prior knowledge: low-rank coding for patterns, smoothness and centering constraints for the PSF, and non-negativity for emitters and background. This modularity suggests clear paths for extension. For example, more elaborate PSF models could incorporate depth-dependent aberrations, and emitters could be modeled with additional constraints such as fluorophore blinking statistics or sparsity in specific transform domains.

The framework has several limitations. First, the current implementation is tailored to linear SIM and assumes a relatively simple cosine pattern model plus perturbations. Extending the method to non-linear SIM or more exotic illumination schemes will require careful redesign of the pattern branch. Second, while self-distillation significantly improves robustness at low photon counts, the training and fine-tuning procedures remain computationally demanding, relying on modern GPUs or TPUs [39]. Third, although we observe good generalization across structures and imaging systems, a systematic study of failure modes—particularly in samples that strongly violate the statistics of the training data—will be important for future work.

Beyond SIM, the ideas underlying SIMFormer are applicable to a broad class of inverse problems in optical imaging, where forward models are well understood but reconstruction is ill-posed. By combining flexible learned priors with explicit physical models and self-supervision, similar architectures could be developed for applications such as light-sheet microscopy, adaptive optics, or computational phase imaging [5, 30]. Finally, the relationship between SIMFormer’s reconstruction error and information-theoretic bounds, such as the Cramér–Rao lower bound, remains an open question. Analyzing this relationship would clarify how close data-driven priors can bring practical reconstruction performance to fundamental physical limits.

## Materials and Methods

### Encoder and decoder

As schematically illustrated in Fig. 1 and Extended Data Fig. 1, the encoder is designed to process raw SIM images and is inspired by spatiotemporal masked autoencoders [17]. A ViT-based encoder with pre-trained CLIP weights [15, 28] processes multi-frame SIM images. To speed up training and improve extraction of fine-grained features, we incorporate a ViT-adapter [27].

Multi-frame SIM images are converted into multiple 768-dimensional vectors via 3D patch embedding. In parallel, the original images are processed through a CNN-based stem, yielding an equal number of 768-dimensional vectors per patch. Both sets are subjected to the same random masking. Unmasked patches are combined with learnable position and frame embeddings, shuffled, and fed into encoder and adapter layers, enabling interaction and information exchange. The encoder output is projected to lower-dimensional vectors per patch; a learnable token replaces masked patches. These features are reordered, combined with positional embeddings, and fed into a decoder consisting of multiple Transformer layers, whose outputs feed three prediction heads.

## Prediction modules for emitters and background

Emitters and background are predicted by a CNN-based module with four blocks, each performing two-fold upsampling. Within each block, upsampling is followed by three  $3 \times 3$  convolutions with Gaussian error linear unit (GELU) activations. The module starts with 512 channels and halves the channel count at each block; a final  $1 \times 1$  convolution produces a single-channel output.

The emitter prediction branch consists of this module followed by a Softplus activation to enforce non-negative outputs. The background branch uses the same module followed by an average pooling layer with kernel size 64, reflecting the assumption that the background varies slowly in space.

## Light pattern reconstruction via low-rank coding

In SIM, the light pattern consists of only a few modes. A typical SIM experiment uses cosine patterns in three directions with three phases per direction, corresponding to nine distinct modes [4, 23]. To encode this prior knowledge, we use low-rank encoding via average pooling. Decoder features are first passed through a Transformer layer, then through one-dimensional average pooling applied to each feature vector, and finally through another Transformer layer to produce the light pattern output.

A common assumption is that the sum of all light patterns in a SIM experiment yields uniform illumination [23]. To ensure that the sum equals one and intensities remain non-negative, we apply a softmax operation along the channel dimension. During multi-stage training, the effective rank of the pattern representation is gradually reduced, biasing the solution towards simpler, more interpretable patterns while preserving the ability to capture experimental deviations from ideal cosines.

## PSF prediction

The PSF prediction module is a CNN that maps a fixed random tensor to the PSF. Following the idea of Deep Image Prior [29], the network recasts PSF estimation as an optimization problem within a neural network, and has been shown to learn PSFs directly from raw microscopy images [30]. We incorporate total-variation regularization on the PSF to encourage smoothness and penalize unphysical oscillations. A centering loss aligns the intensity-weighted PSF centroid with the geometric center of the tensor, preventing drift during training.

## Loss function

The loss function combines several terms to enable self-supervised learning from raw SIM images. The first category measures differences between reconstructed and raw SIM images, using an  $L_1$  distance and MS-SSIM; their weighted average is known to be effective for image restoration [32]. The second category includes: (1) a center-distance term enforcing alignment between the intensity-weighted PSF center and tensor center; and (2) total-variation losses on PSF and light patterns to encourage spatial smoothness. The overall loss is a weighted sum of these terms, with hyperparameters chosen to balance data fidelity and regularization across synthetic and real datasets.

## Training procedure

Training begins from a pre-trained CLIP-based initialization [28], since training ViTs from scratch on small datasets is suboptimal [16]. Initial training uses batch size 96, 70 epochs, patch size  $3 \times 16 \times 16$ , and mask ratio 0.75. A multi-stage schedule then gradually compresses the light

pattern rank from 512 to 32 (256, 128, 64, 32), with each stage using mask ratio 0.25, batch size 64, and 30 epochs. After reaching rank 32, we train for 2000 epochs with batch size 96 and mask ratio 0.25 for synthetic data / 0.75 for BioSR.

Throughout, patch size  $3 \times 16 \times 16$ , crop size  $80 \times 80$ , PSF size  $49 \times 49$ , and learning rate  $10^{-4}$  are maintained. Raw images are linearly scaled by a factor of three, yielding threefold-enlarged SIM reconstructions; unscaled raw images are used in the loss to maintain physical consistency with the forward model.

## Self-distillation

To obtain SIMFormer+, we perform self-distillation. SIMFormer is first trained on high-SNR SIM images, producing high-resolution predictions. These are then used as soft labels to train SIMFormer+ under lower photon counts and higher noise. High-SNR versions of test images are excluded from both training sets to avoid information leakage. SIMFormer+ thus inherits high-resolution capabilities while greatly improving noise robustness [18, 20, 21]. In practice, we observe that SIMFormer+ suppresses spurious high-frequency artifacts that sometimes appear in the teacher’s predictions when photon counts are extremely low.

## Normalization

We apply percentile-based normalization to both ground truth and reconstructed images:

$$I_{\text{norm}} = \frac{I - \text{Percentile}(I, 0.1)}{\text{Percentile}(I, 99.9) - \text{Percentile}(I, 0.1)}.$$

This ensures consistent dynamic ranges across images and reduces sensitivity to outliers and hot pixels. All metrics (NRMSE, MS-SSIM) are computed on normalized images.

## Decorrelation analysis

Resolution is assessed via decorrelation analysis [34], which identifies the highest spatial frequency by examining local peaks in decorrelation functions, rather than relying on Abbe’s criterion. Briefly, the decorrelation function is computed in the Fourier domain and radial profiles are extracted. Local maxima in these profiles correspond to effective resolution limits. We follow the procedure described in Ref. [34] and apply it uniformly to all reconstruction methods for fair comparison.

## Computational resources and speed

We implement SIMFormer in JAX [39], training on eight NVIDIA Tesla A100 80 GB GPUs for seven days (24 hours/day). Inference for a single SIM stack of shape (9, 512, 512) takes approximately one second. All experiments are performed using mixed-precision training to reduce memory consumption and accelerate convergence.

## Acknowledgments

**Funding.** Fang-Wen Sun and Xiang-Dong Chen were supported by the National Natural Science Foundation of China (No. 62225506), CAS Project for Young Scientists in Basic Research (No. YSBR-049), and the Innovation Program for Quantum Science and Technology (No. 2021ZD0303200). Xiang-Dong Chen was also supported by the Key Research and Development Program of Anhui Province (No. 2022b13020006).

**Author contributions.** Z. W. conceived the project. F. S. and T. C. supervised the research. Z. W., F. S., and T. C. designed the experiments. T. W. and Z. W. performed experiments. Z. W., F. S., and T. C. wrote the manuscript. All authors discussed the results and commented on the manuscript.

**Competing interests.** The authors declare no conflict of interest.

**Data availability.** Data supporting the findings of this study are available from the corresponding author upon reasonable request.

**Use of large language models.** Portions of this manuscript were edited for grammar and stylistic consistency with the assistance of a large-language-model service. The tool was used only for language polishing; it did not generate research content, analysis, or conclusions. All edits were individually reviewed and approved by the authors, who remain fully responsible for the accuracy and integrity of the work.

## References

- [1] Stefan W. Hell and Jan Wichmann. Breaking the diffraction resolution limit by stimulated emission: stimulated-emission-depletion fluorescence microscopy. *Optics Letters*, 19:780–782, 1994.
- [2] M. J. Rust, M. Bates, and X. Zhuang. Sub-diffraction-limit imaging by stochastic optical reconstruction microscopy (storm). *Nature Methods*, 3:793–796, 2006.
- [3] S. Manley et al. High-density mapping of single-molecule trajectories with photoactivated localization microscopy. *Nature Methods*, 5:155–157, 2008.
- [4] M. G. L. Gustafsson. Surpassing the lateral resolution limit by a factor of two using structured illumination microscopy. *Journal of Microscopy*, 198:82–87, 2000.
- [5] W. Tian, R. Chen, and L. Chen. Computational super-resolution: An odyssey in harnessing priors to enhance optical microscopy resolution. *Analytical Chemistry*, 97:4763–4792, 2025.
- [6] S. Farsiu, M. D. Robinson, M. Elad, and P. Milanfar. Fast and robust multiframe super resolution. *IEEE Transactions on Image Processing*, 13:1327–1344, 2004.
- [7] C. Bouman and K. Sauer. A generalized gaussian image model for edge-preserving map estimation. *IEEE Transactions on Image Processing*, 2:296–310, 1993.
- [8] N. Dey et al. Richardson–lucy algorithm with total variation regularization for 3d confocal microscope deconvolution. *Microscopy Research and Technique*, 69:260–266, 2006.
- [9] W. Zhao et al. Sparse deconvolution improves the resolution of live-cell super-resolution fluorescence microscopy. *Nature Biotechnology*, 40:606–617, 2022.
- [10] X. Chen et al. Superresolution structured illumination microscopy reconstruction algorithms: a review. *Light: Science & Applications*, 12:172, 2023.
- [11] C. Belthangady and L. A. Royer. Applications, promises, and pitfalls of deep learning for fluorescence image reconstruction. *Nature Methods*, 16:1215–1225, 2019.
- [12] L. Jin et al. Deep learning enables structured illumination microscopy with low light levels and enhanced speed. *Nature Communications*, 11:1934, 2020.
- [13] C. Qiao et al. Evaluation and development of deep neural networks for image super-resolution in optical microscopy. *Nature Methods*, 18:194–202, 2021.
- [14] A. Vaswani et al. Attention is all you need. In *Advances in Neural Information Processing Systems*, volume 30, pages 5998–6008, 2017.
- [15] A. Dosovitskiy et al. An image is worth 16x16 words: Transformers for image recognition at scale. In *International Conference on Learning Representations*, 2021.
- [16] K. He et al. Masked autoencoders are scalable vision learners. In *Proceedings of the IEEE/CVF Conference on Computer Vision and Pattern Recognition*, pages 16000–16009, 2022.
- [17] C. Feichtenhofer, H. Fan, Y. Li, and K. He. Masked autoencoders as spatiotemporal learners. In *Advances in Neural Information Processing Systems*, volume 35, pages 35946–35958, 2022.

- [18] L. Zhang et al. Be your own teacher: Improve the performance of convolutional neural networks via self distillation. In *Proceedings of the IEEE/CVF International Conference on Computer Vision*, pages 3713–3722, 2019.
- [19] G. Hinton, O. Vinyals, and J. Dean. Distilling the knowledge in a neural network. arXiv preprint arXiv:1503.02531, 2015.
- [20] L. Zhang, C. Bao, and K. Ma. Self-distillation: Towards efficient and compact neural networks. *IEEE Transactions on Pattern Analysis and Machine Intelligence*, 44:4388–4403, 2022.
- [21] M. Pham, M. Cho, A. Joshi, and C. Hegde. Revisiting self-distillation. arXiv preprint arXiv:2206.08491, 2022.
- [22] Q. Zhang, Y. Wang, and Y. Wang. How mask matters: Towards theoretical understandings of masked autoencoders. In *Advances in Neural Information Processing Systems*, volume 35, pages 27127–27139, 2022.
- [23] E. Mudry et al. Structured illumination microscopy using unknown speckle patterns. *Nature Photonics*, 6:312–315, 2012.
- [24] Z. H. Shah et al. Evaluation of swin transformer and knowledge transfer for denoising of super-resolution structured illumination microscopy data. *Gigascience*, 13:giad109, 2024.
- [25] X. Chen et al. Self-supervised denoising for multimodal structured illumination microscopy enables long-term super-resolution live-cell imaging. *Photonix*, 5:4, 2024.
- [26] Z. Burns and Z. Liu. Untrained, physics-informed neural networks for structured illumination microscopy. *Optics Express*, 31:8714–8724, 2023.
- [27] Z. Chen et al. Vision transformer adapter for dense predictions. In *International Conference on Learning Representations*, 2023.
- [28] A. Radford et al. Learning transferable visual models from natural language supervision. In *Proceedings of the 38th International Conference on Machine Learning*, pages 8748–8763, 2021.
- [29] D. Ulyanov, A. Vedaldi, and V. Lempitsky. Deep image prior. In *Proceedings of the IEEE/CVF Conference on Computer Vision and Pattern Recognition*, pages 9446–9454, 2018.
- [30] Z.-H. Wang et al. Learning the imaging mechanism directly from optical microscopy observations. *Photonics Research*, 12:7–26, 2024.
- [31] Y. Bengio, J. Louradour, R. Collobert, and J. Weston. Curriculum learning. In *Proceedings of the 26th International Conference on Machine Learning*, pages 41–48. ACM, 2009.
- [32] H. Zhao, O. Gallo, I. Frosio, and J. Kautz. Loss functions for image restoration with neural networks. *IEEE Transactions on Computational Imaging*, 3:47–57, 2016.
- [33] B. Wang, Z. Zhao, M. Xiong, R. Yan, and K. Xu. The endoplasmic reticulum adopts two distinct tubule forms. *Proceedings of the National Academy of Sciences*, 119:e2117559119, 2022.
- [34] A. Descloux, K. S. Grußmayer, and A. Radenovic. Parameter-free image resolution estimation based on decorrelation analysis. *Nature Methods*, 16:918–924, 2019.

- [35] M. Müller, V. Mönkemöller, S. Hennig, W. Hübner, and T. Huser. Open-source image reconstruction of super-resolution structured illumination microscopy data in imagej. *Nature Communications*, 7:10980, 2016.
- [36] H. T. McMahon and E. Boucrot. Molecular mechanism and physiological functions of clathrin-mediated endocytosis. *Nature Reviews Molecular Cell Biology*, 12:517–533, 2011.
- [37] A. Desai and T. J. Mitchison. Microtubule polymerization dynamics. *Annual Review of Cell and Developmental Biology*, 13:83–117, 1997.
- [38] G. M. Cooper and K. Adams. *The Cell: A Molecular Approach*. Oxford University Press, Oxford, UK, 2022.
- [39] J. Bradbury et al. Jax: Composable transformations of python+numpy programs. arXiv preprint arXiv:1804.00289, 2018.

# Figures

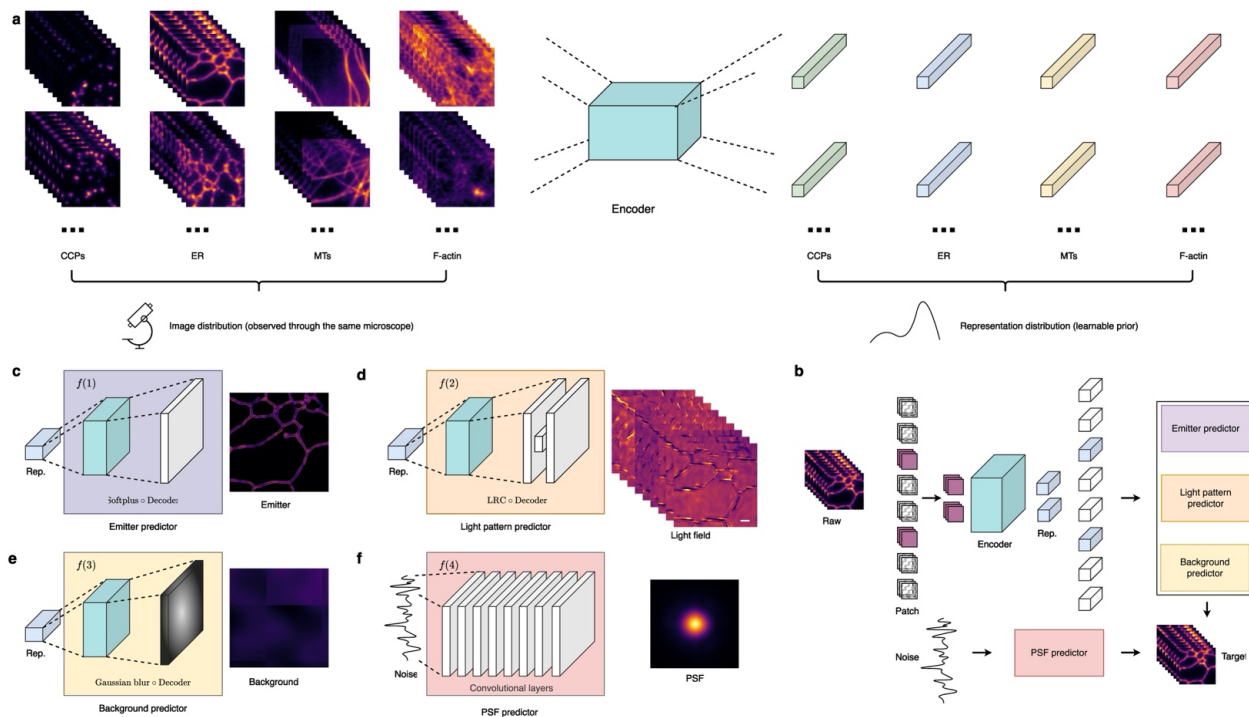


Fig. 1. Overview of SIMFormer. (A) The image encoder extracts representations from SIM raw images and is updated through self-supervised training. (B) SIMFormer is a self-supervised learning architecture based on masked autoencoders. (C) The representation is mapped to emitters using the decoder and Softplus activation. (D) The representation is mapped to light patterns using the decoder and low-rank coding (LRC). (E) The representation is mapped to the background using the decoder and Gaussian blur. (F) The PSF is generated from fixed noise using a convolutional network.

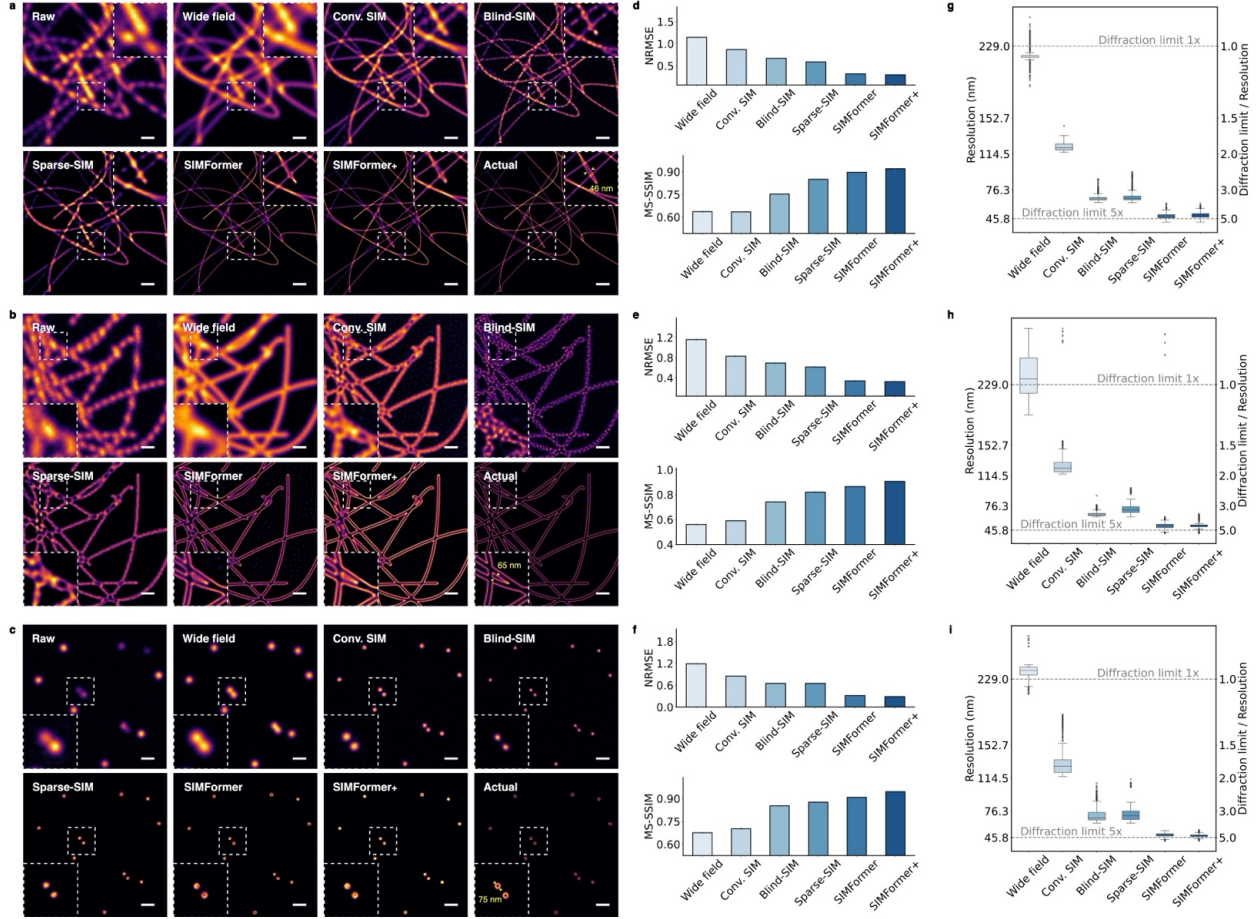


Fig. 2. Evaluation of estimated emitters for synthetic data. (A–C) Visual comparison of the super-resolution reconstruction of conventional SIM, Sparse-SIM, Blind-SIM, SIMFormer, and SIMFormer+ on the raw SIM images. (D–F) Quantitative analysis results using NRMSE and MS-SSIM. (G–I) Resolution obtained from the decorrelation analysis. (A) Visualization results of emitters with synthetic filament structures. (B) Visualization results of emitters with synthetic microtubule structures. (C) Visualization results for emitters with synthetic ring structures. Scale bar: 0.5  $\mu\text{m}$ . (D) NRMSE and MS-SSIM results of synthetic filament emitters. (E) NRMSE and MS-SSIM results of synthetic microtubular emitters. (F) NRMSE and MS-SSIM results of synthetic ring structure emitters. (G) Resolution of estimated emitters with synthetic filament structures. (H) Resolution of estimated emitters with synthetic microtubule structures. (I) Resolution of estimated emitters with synthetic ring structures. Box plots show the median (centre line), 25th–75th percentiles (box), and  $1.5 \times \text{IQR}$  whiskers; outliers are plotted as dots.

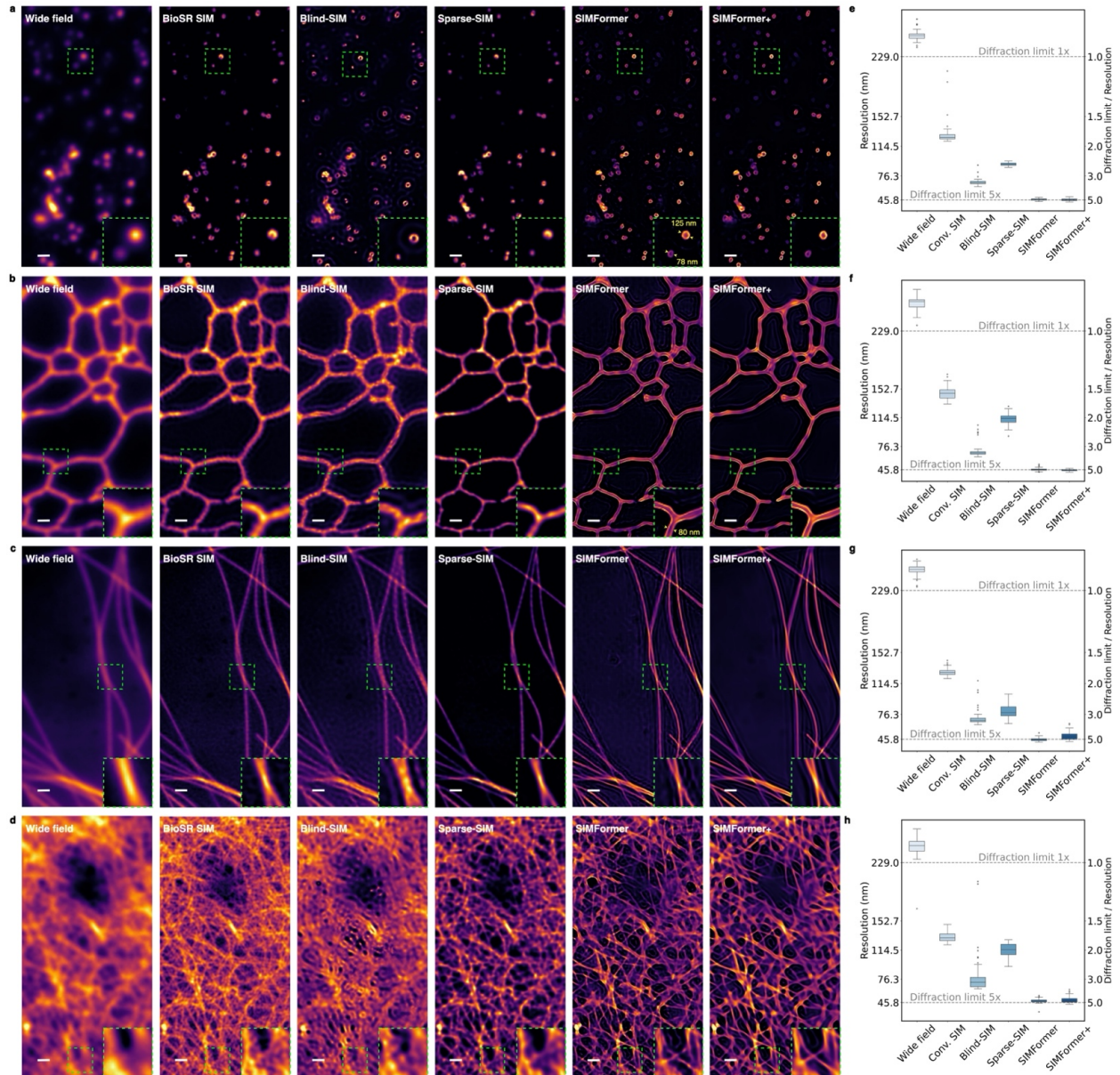


Fig. 3. Experiments on the BioSR dataset. (A–D) Visualization results of the BioSR data from wide field imaging, BioSR SIM, Blind-SIM, SIMFormer, and SIMFormer+. (E–H) Resolution obtained from decorrelation analysis. (A) Comparison results for ER. (B) Comparison results for CCPs. (C) Comparison results for MTs. (D) Comparison results for F-actin. Scale bar: 0.5  $\mu\text{m}$ . (E) Resolution for ER. (F) Resolution for CCPs. (G) Resolution for MTs. (H) Resolution for F-actin. Box plots show the median (centre line), 25th–75th percentiles (box), and  $1.5 \times \text{IQR}$  whiskers; outliers are plotted as dots.

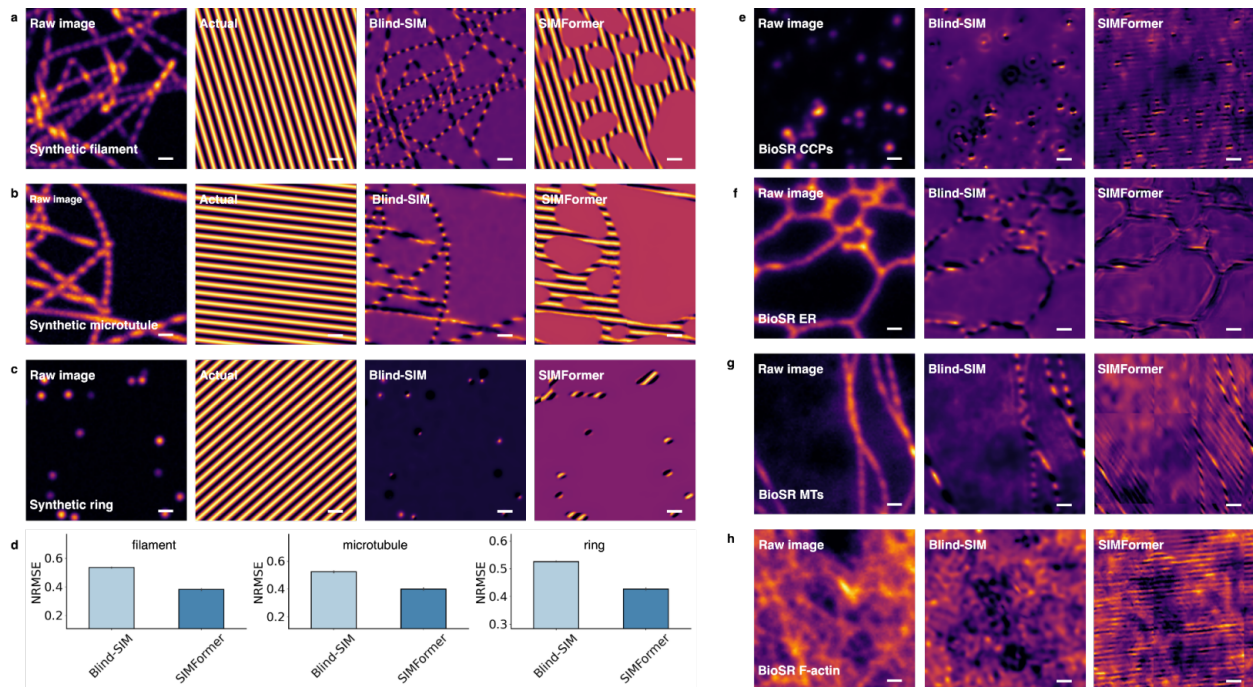


Fig. 4. Light pattern estimation. (A–C) Comparison of estimated light patterns from synthetic data. The emitters are (A) synthetic filament, (B) synthetic microtubule, and (C) synthetic ring. (D) Quantitative evaluation of the light pattern using NRMSE. (E–H) Comparison of estimated light patterns from BioSR data. The emitters are (E) CCPs, (F) ER, (G) MTs, and (H) F-actin.

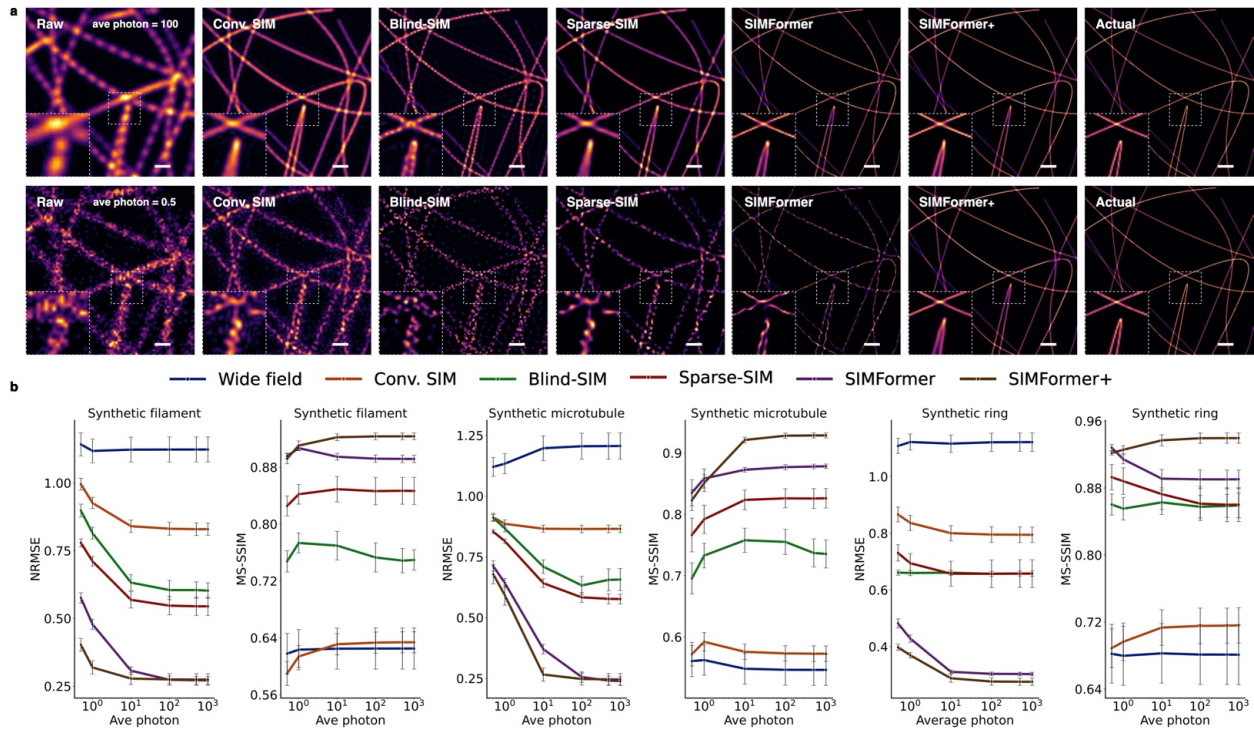


Fig. 5. Noise robustness of synthetic data. Comparison of the super-resolution reconstruction of conventional SIM, Sparse-SIM, Blind-SIM, SIMFormer, and SIMFormer+ on the raw SIM images with average photon count equal to 0.5, 1, 10, 100, 500, and 1000. (A) Comparative presentation of high and low photon-number results for synthetic filaments. (B) Quantitative evaluation using NRMSE and MS-SSIM. Scale bar: 0.5  $\mu\text{m}$ . Lines represent the mean; error bars denote the standard error of the mean.

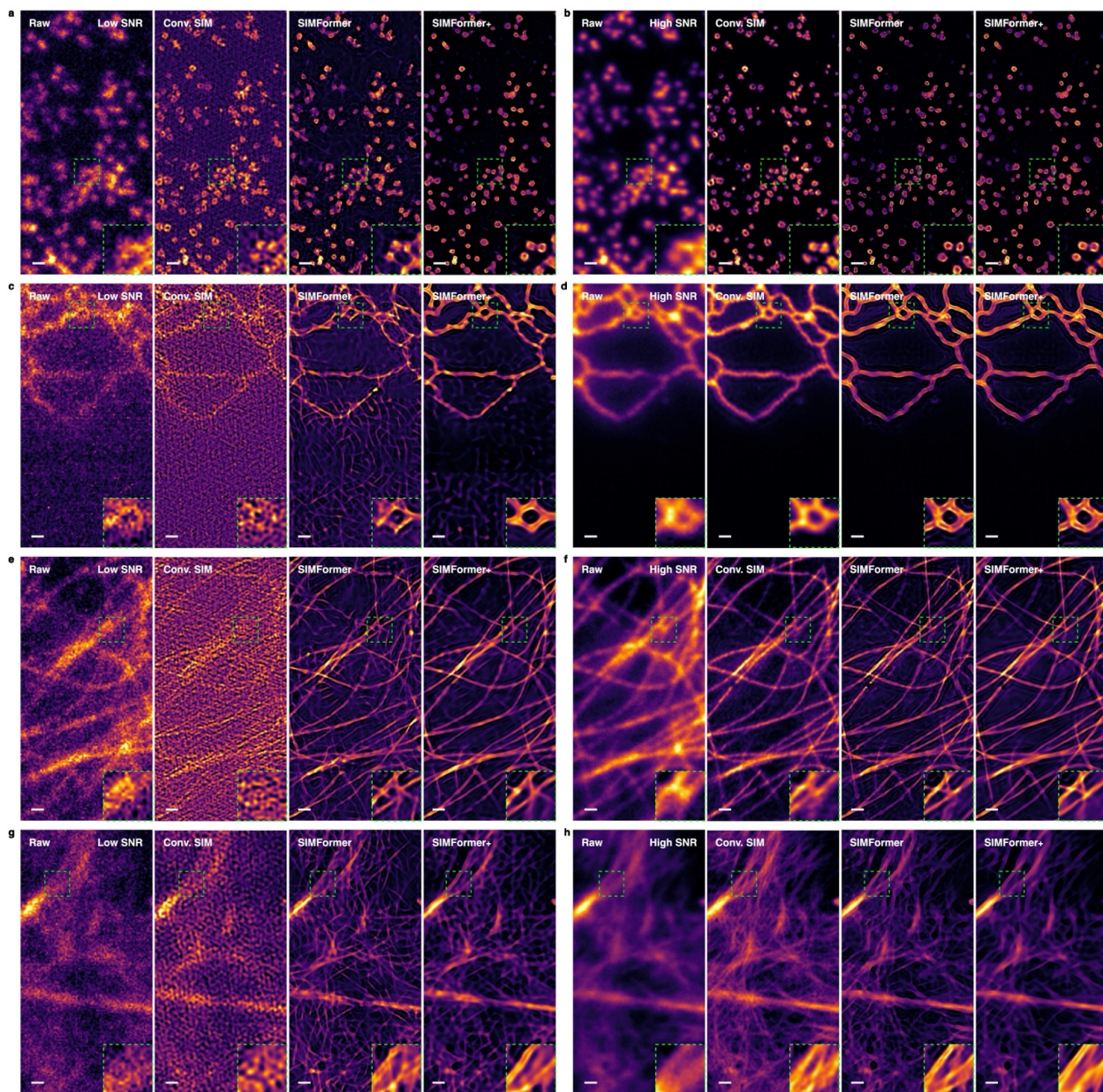
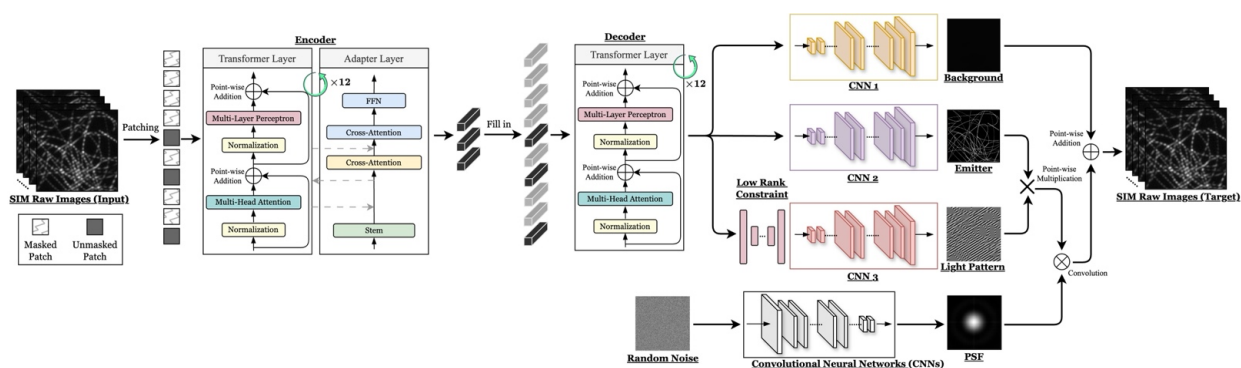
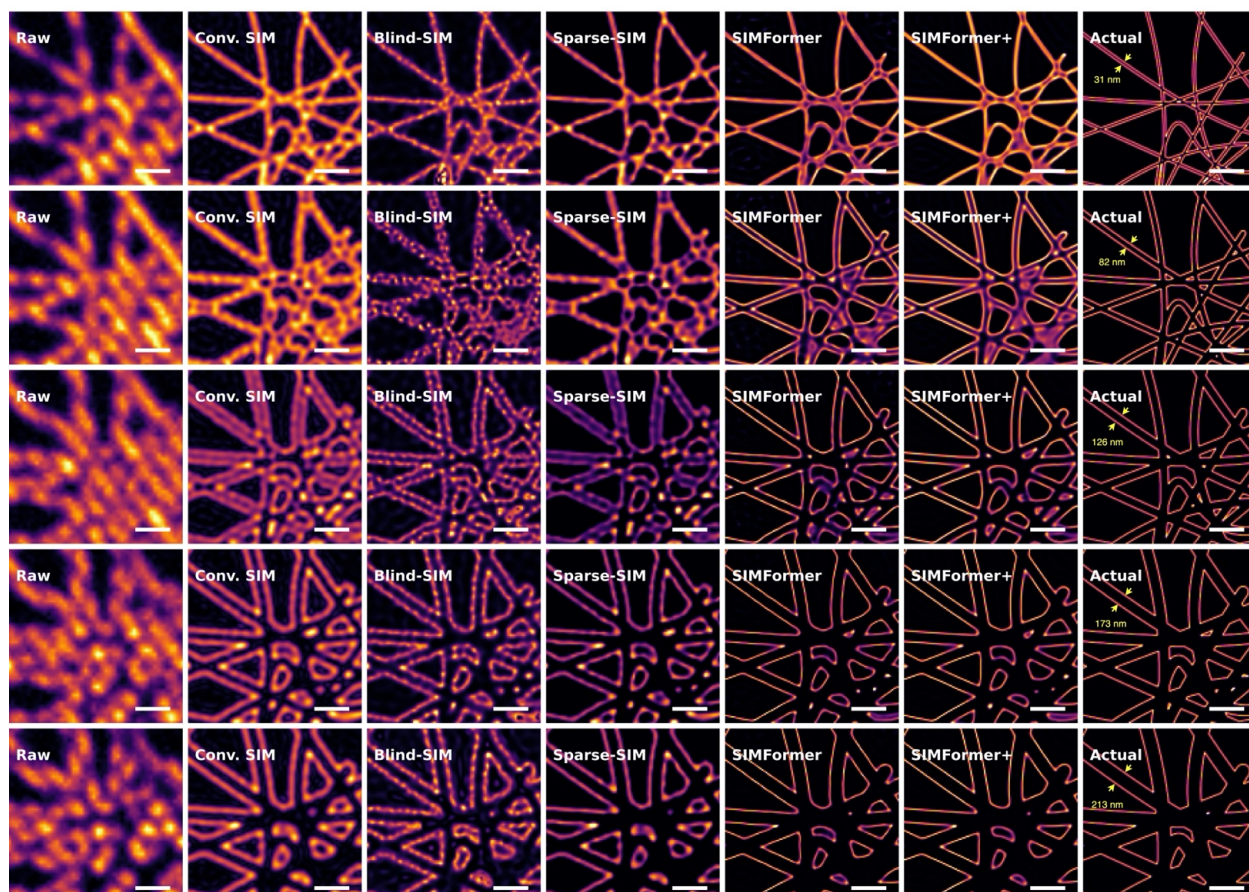


Fig. 6. Noise robustness on BioSR data. Comparison of SIM raw images, conventional SIM reconstruction, and SIMFormer+ with low signal-to-noise ratio (SNR) and high SNR. The raw images are (A) CCPs with low SNR, (B) CCPs with high SNR, (C) ER with low SNR, (D) ER with high SNR, (E) MTs with low SNR, (F) MTs with high SNR, (G) F-actin with low SNR, and (H) F-actin with high SNR. Scale bar: 0.5  $\mu\text{m}$ .

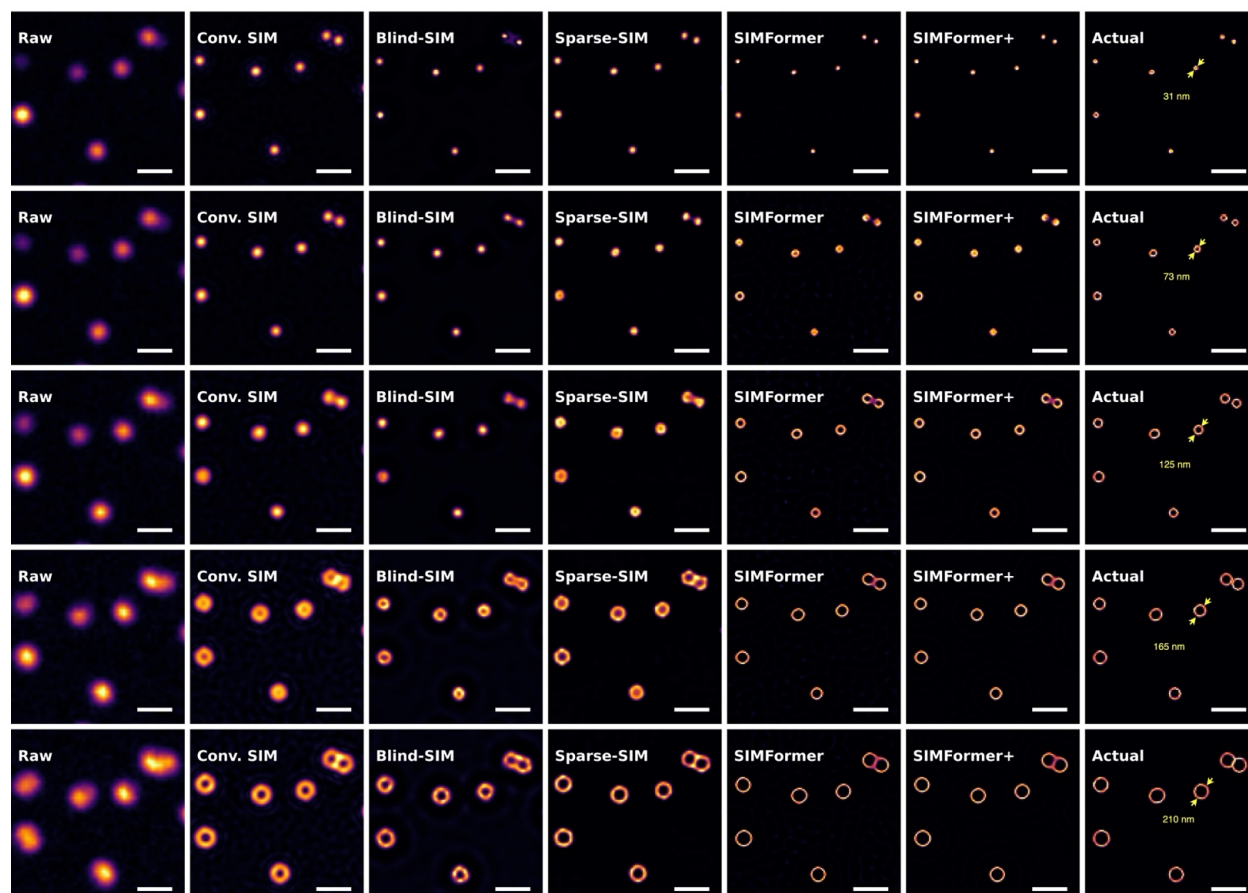
## Extended Data Figures



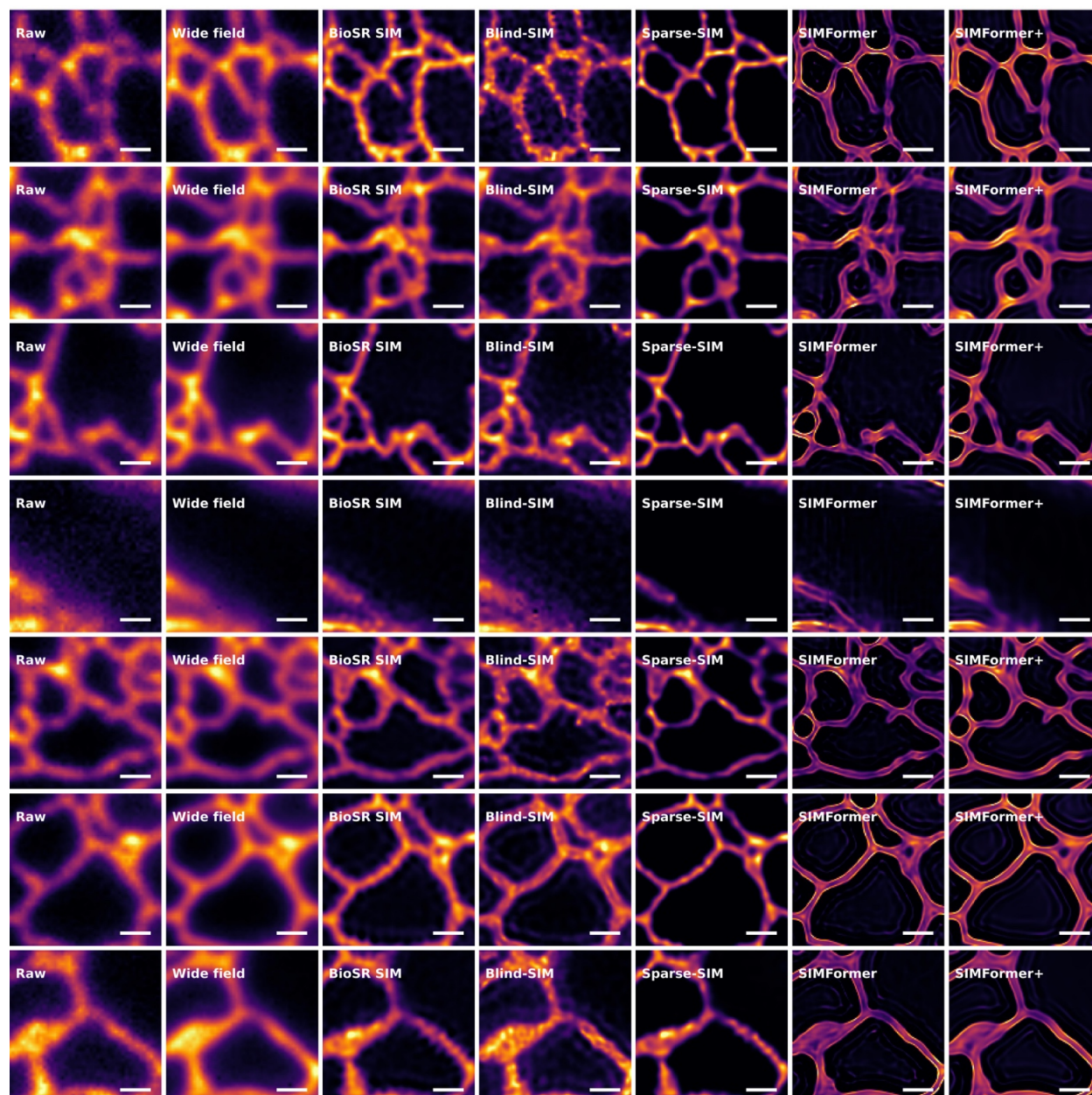
Extended Data Fig. 1. Network architecture of SIMFormer. The input is raw SIM images, and the output includes the background, emitters, light pattern, and PSF. The design uses a masked autoencoder with a transformer encoder, an adapter, and a transformer + CNN decoder.



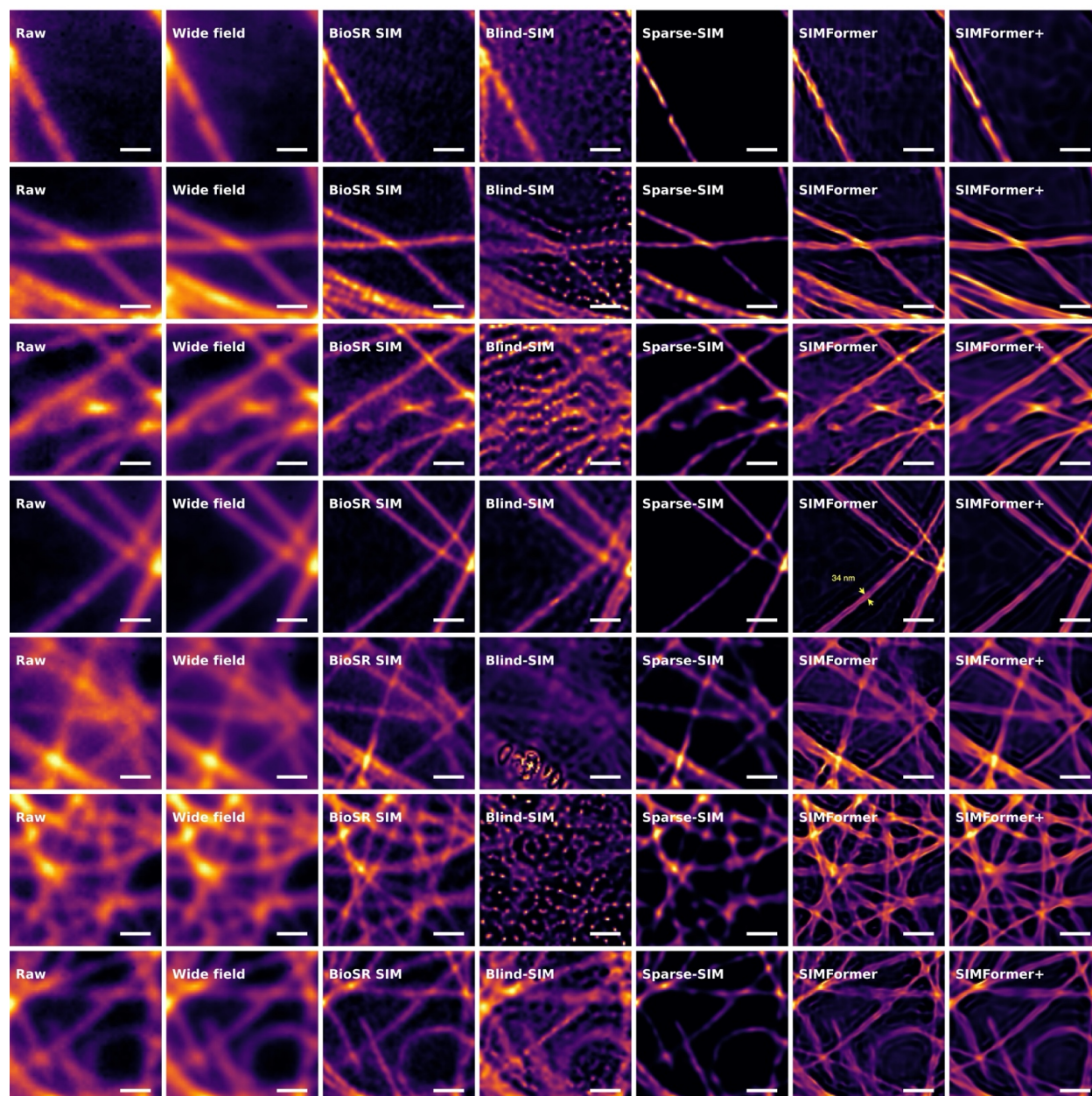
Extended Data Fig. 2. Representative synthetic microtubule structures results. Comparison of wide-field results, conventional SIM results, Blind-SIM results, Sparse-SIM results, SIMFormer results, and SIMFormer+ results. From top to bottom represents a gradual increase in microtubule width. Scale bar: 0.5  $\mu\text{m}$ .



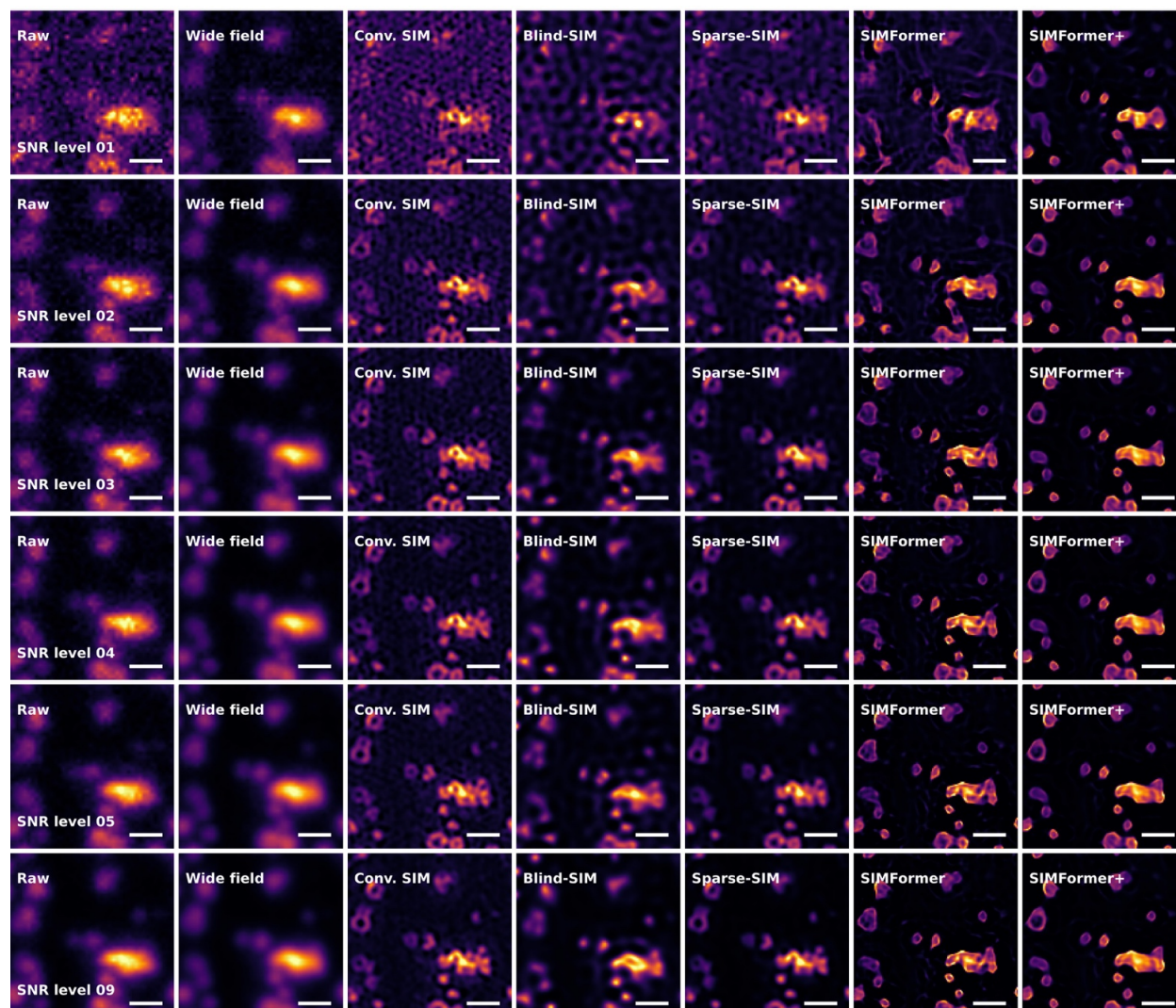
Extended Data Fig. 3. Representative synthetic ring structure results. Comparison of wide-field results, conventional SIM results, Blind-SIM results, Sparse-SIM results, SIMFormer results, and SIMFormer+ results. From top to bottom represents a gradual increase in the radius of the ring. Scale bar: 0.5  $\mu\text{m}$ .



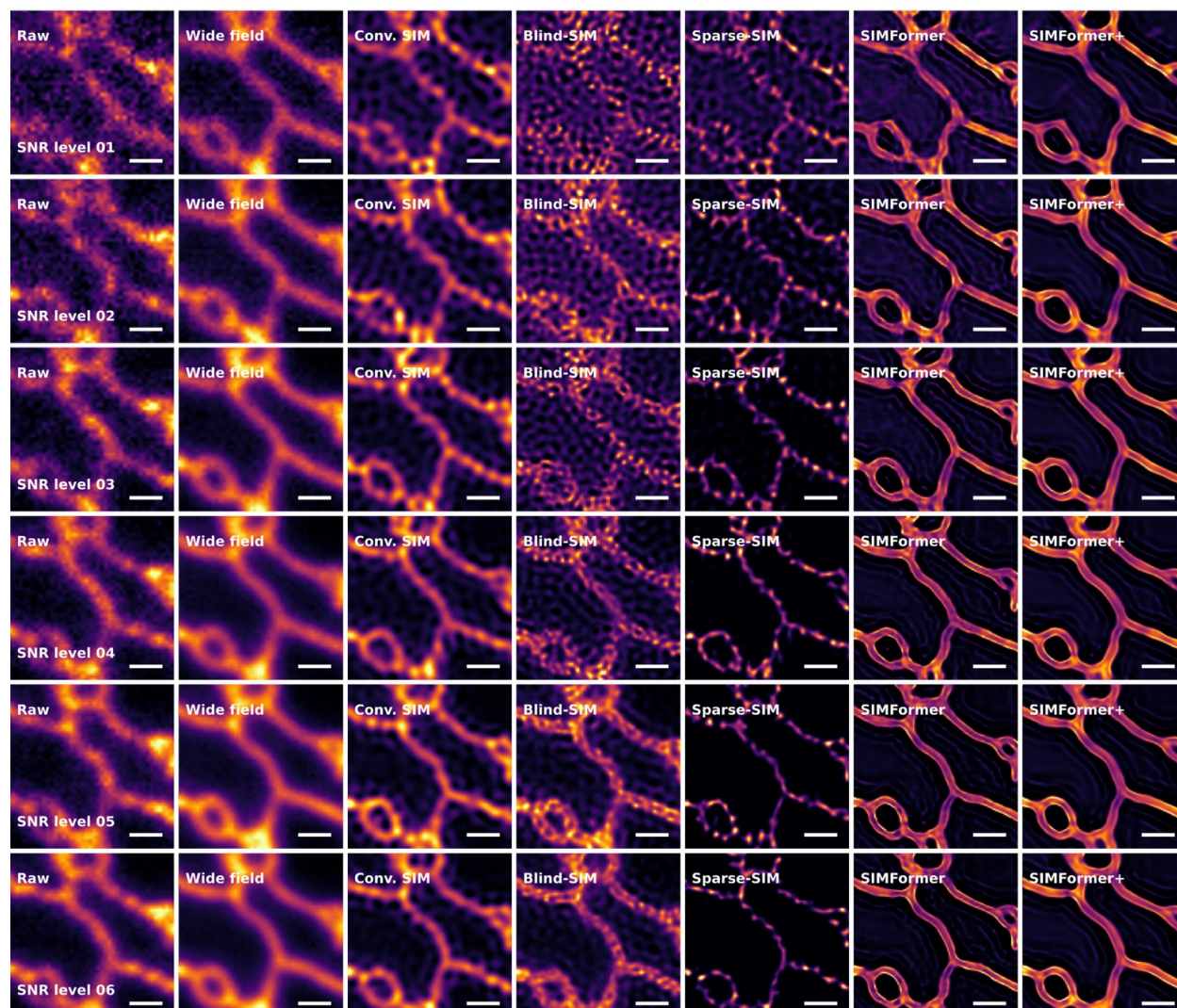
Extended Data Fig. 4. Representative ER results. Comparison of wide-field results, SIM results (BioSR), Blind-SIM results, Sparse-SIM results, SIMFormer results, and SIMFormer+ results. Scale bar: 0.5  $\mu\text{m}$ .



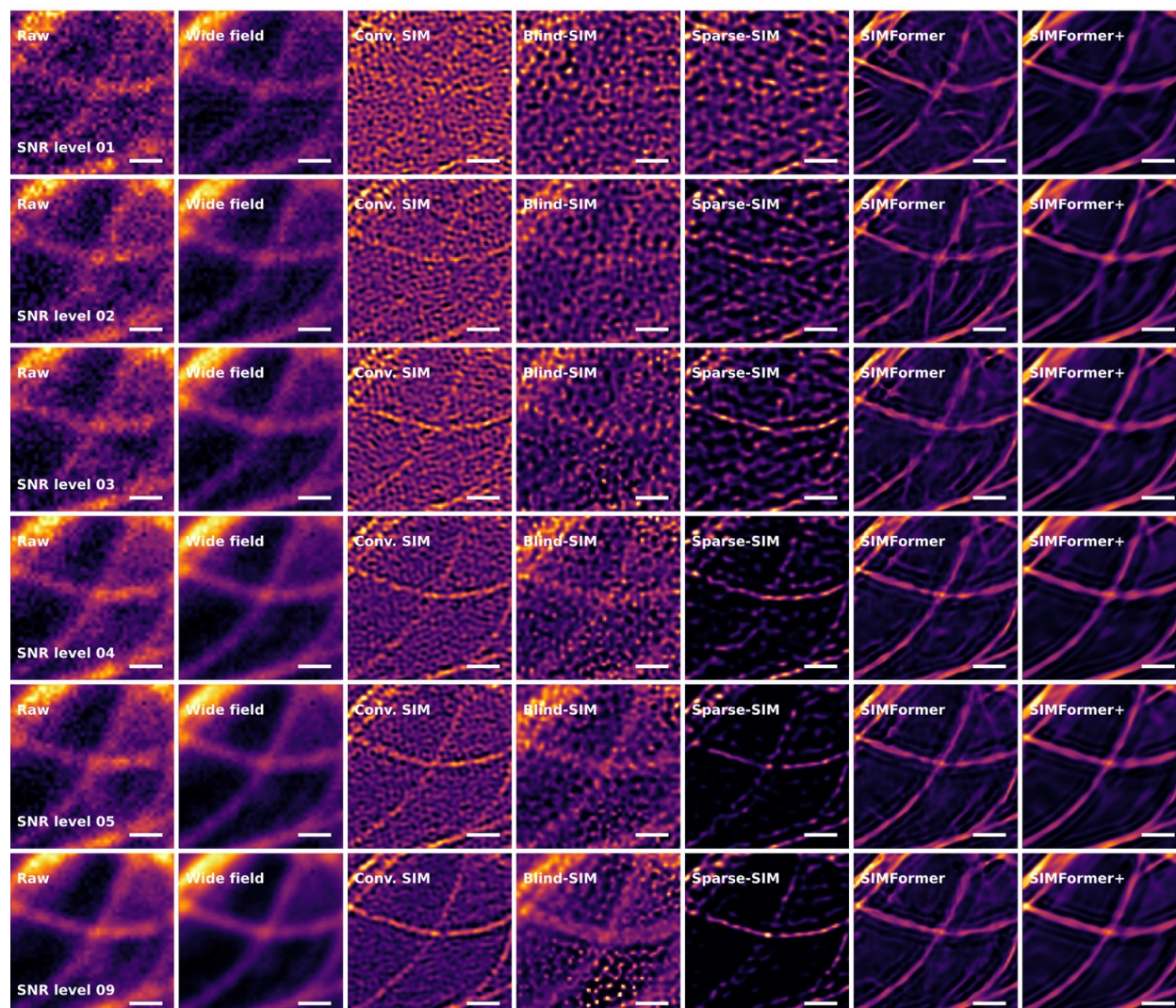
Extended Data Fig. 5. Representative MTs results. Comparison of wide-field results, SIM results (BioSR), Blind-SIM results, Sparse-SIM results, SIMFormer results, and SIMFormer+ results. Scale bar: 0.5  $\mu\text{m}$ .



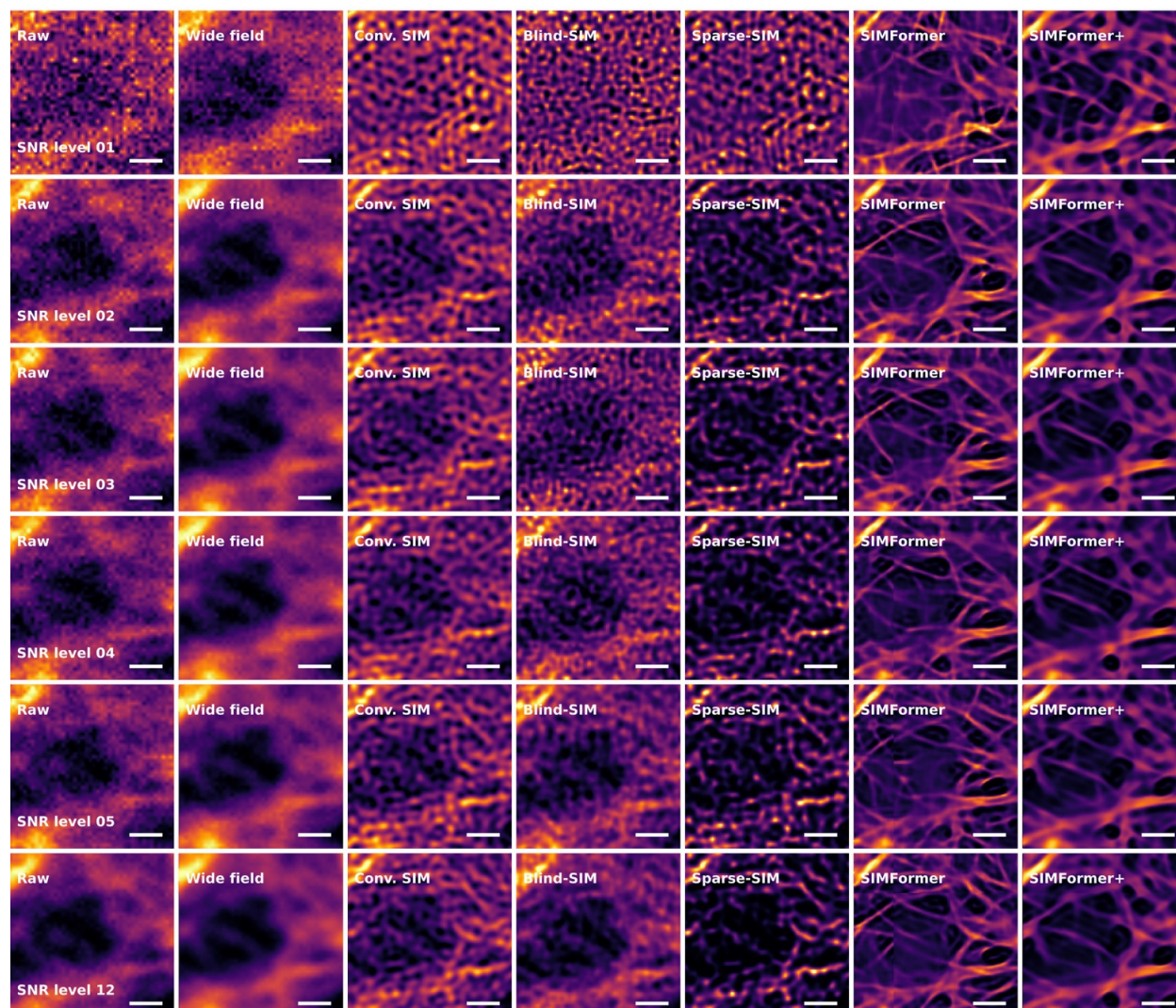
Extended Data Fig. 6. Noise robustness of CCPs data. Comparison of noise robustness among wide-field results, SIM results (fairSIM), Blind-SIM results, Sparse-SIM results, SIMFormer results, and SIMFormer+ results. Scale bar: 0.5  $\mu\text{m}$ .



Extended Data Fig. 7. Noise robustness of ER data. Comparison of noise robustness among wide-field results, SIM results (fairSIM), Blind-SIM results, Sparse-SIM results, SIMFormer results, and SIMFormer+ results. Scale bar: 0.5  $\mu\text{m}$ .



Extended Data Fig. 8. Noise robustness of MTs data. Comparison of noise robustness among wide-field results, SIM results (fairSIM), Blind-SIM results, Sparse-SIM results, SIMFormer results, and SIMFormer distilled results. Scale bar: 0.5  $\mu\text{m}$ .



Extended Data Fig. 9. Noise robustness of F-actin data. Comparison of noise robustness among wide-field results, SIM results (fairSIM), Blind-SIM results, Sparse-SIM results, SIMFormer results, and SIMFormer distilled results. Scale bar: 0.5  $\mu\text{m}$ .